IOPscience iopscience.iop.org

Home Search Collections Journals About Contact us My IOPscience

Electronic properties of the n-type PDI8-CN_2 organic semiconductor at the interface with SiO_2: addressing the role of adsorbed water molecules by means of optical second-harmonic generation

This content has been downloaded from IOPscience. Please scroll down to see the full text.

2014 New J. Phys. 16 093036

(http://iopscience.iop.org/1367-2630/16/9/093036)

View the table of contents for this issue, or go to the journal homepage for more

Download details:

IP Address: 61.178.182.134
This content was downloaded on 25/08/2015 at 15:31

Please note that terms and conditions apply.

New Journal of Physics
The open access journal at the forefront of physics
Deutsche Physikalische Gesellschaft DPG | IOP Institute of Physics

Electronic properties of the n-type PDI8-CN_2 organic semiconductor at the interface with SiO_2: addressing the role of adsorbed water molecules by means of optical second-harmonic generation

F Ciccullo[1,2], L Santamaria[2,3], E Orabona[1,2], A Cassinese[1,2], P Maddalena[1,2] and S Lettieri[1]

[1] Institute for Superconductors, Oxides and Innovative Materials, National Research Council (CNR-SPIN), U.O.S. Napoli, Via Cintia, I-80126 Napoli, Italy
[2] Physics Department, University of Naples Federico II, Via Cintia I-80126 Napoli, Italy
E-mail: stefano.lettieri@spin.cnr.it

Received 21 January 2014, revised 11 July 2014
Accepted for publication 16 July 2014
Published 24 September 2014

New Journal of Physics **16** (2014) 093036

doi:10.1088/1367-2630/16/9/093036

Abstract

We investigate the interfacial electronic properties of N,N'-bis(n-octyl)-(1,7&1,6)-dicyanoperylene-3,4:9,10-bisdicarboximide (PDI8-CN_2) organic semiconductor films grown on silicon dioxide (SiO_2) by polarization-resolved second harmonic generation optical spectroscopy. The analysis shows a non-uniform distribution of charge carriers in PDI8-CN_2, whose spatial profile is affected by hydrophobic passivation of SiO_2 surfaces by hexamethyldisilazane. An interpretation model strengthened by photoluminescence analysis is developed, based on the presence of the net charge localized at the SiO_2 surface and on consequent charge redistribution in the organic semiconductor. Considerations are expounded suggesting a common and 'universal' mechanism for the bias stress effect in p-channel and n-channel organic field-effect transistors, related to proton migration toward SiO_2 gate dielectrics.

[3] Present address: INO-CNR, Istituto Nazionale di Ottica, Sezione di Napoli, Via Campi Flegrei 34, I-80078 Pozzuoli (NA), Italy.

Content from this work may be used under the terms of the Creative Commons Attribution 3.0 licence. Any further distribution of this work must maintain attribution to the author(s) and the title of the work, journal citation and DOI.

© 2014 IOP Publishing Ltd and Deutsche Physikalische Gesellschaft

S Online supplementary data available from stacks.iop.org/njp/16/093036/mmedia

Keywords: organic semiconductors, interface properties, nonlinear optical spectroscopy, organic electronics, organic field-effect transistors, surface optics

1. Introduction

The progress in organic electronics is closely related to the ability to analyze and predict the electronic properties of interfaces playing a role in the devices [1, 2]. This is particularly evident in the case of organic field-effect transistors (OFETs), whose performances are definitely affected by local interactions of the organic semiconductor at the interface with the gate dielectric [3–9] and/or air [10–12]. Optical spectroscopy can provide direct and contact-free probing of the electronic properties of organic semiconductors [13, 14], but unfortunately the most commonly used optical techniques are not spatially-selective, as they are based on *linear* matter–radiation interaction processes occurring in the whole medium (e.g. absorption, reflection, fluorescence). In light of the aforementioned considerations, exploitation of optical processes characterized by an intrinsic sensitivity to the physical state of surfaces/interfaces in organic-based devices is instead desirable.

One example of a spatially-selective optical phenomenon is represented by optical second harmonic generation (SHG), consisting of the generation of an electromagnetic wave of frequency 2ω ('second-harmonic' or SH wave) caused by the interaction between a material medium and a laser beam ('fundamental beam') of frequency ω. In fact, symmetry considerations allow one to demonstrate that such a process cannot take place in material regions where inversion symmetry holds [15]. Thus, SHG analysis allows selective probing of electronic properties in regions where the latter symmetry is broken due to material discontinuities (i.e. surfaces/interfaces) or to the presence of a local field having a well-defined direction. Also thanks to other useful peculiarities (e.g. access to interfaces, absence of physical contacts, the possibility to study dynamic processes by time-resolved detection [16–20]), SHG has been successfully employed in recent years for investigations on carrier mobility [21, 22], channel formation [23], trap states [24] and charge transfer [25] in OFETs and organic heterostructures.

SHG spectroscopy appears to be particularly suited to the study of surface/interface processes in organic polycrystalline films characterized by centrosymmetric structures and by large in-plane charge delocalization[4]. An interesting molecule that forms thin films with such characteristics [30] is PDI8-CN_2 (N,N'-bis(n-octyl)-(1,7&1,6)-dicyanoperylene-3,4:9,10-bisdicarboximide), a perylene diimide derivative considered to be one of the most promising materials for realization of stable n-channel OFETs [26, 27, 29] and complementary circuits [28]. Similarly to many p-channel OFETs, n-channel OFETs based on PDI8-CN_2 and using SiO_2 as the gate dielectric exhibit a bias stress effect (BSE), namely the drift of threshold voltage during prolonged operation. Understanding the origins of such an effect is very

[4] Electronic delocalization over several identical repeat units is a fundamental prerequisite for large $\chi^{(3)}$ EFISHG susceptibilities. In this regard, see [31].

important for future realization of stable and reliable electronic devices based on organic semiconductors.

So far, the study of BSE has mostly been conducted on p-type organic semiconductors. Significant evidence exists indicating that BSE is intimately linked to the presence of water molecules adsorbed on the SiO_2 gate dielectric [32, 33] and that it can be dramatically slowed down through hydrophobic coating of SiO_2 [34, 35]. Recently, a model based on redox reactions taking place at the semiconductor/dielectric interface and accompanied by reversible migration of protons into the gate dielectric has been proposed for p-type organic semiconductors, able to clarify most of the BSE characteristics [36]. However, BSE in n-type organic semiconductors is still an issue deserving more investigation. In particular, the question arises if there is a *common* mechanism driving BSE in all (i.e. p-channel and n-channel as well) kinds of OFETs.

Motivated by these considerations, we report on an SHG analysis—assisted by photoluminescence (PL) investigations—devoted to the study of interfacial electronic properties of PDI8-CN_2 films grown on both bare and hexamethyldisilazane (HMDS)-treated SiO_2 substrates. By analyzing a set of variable thickness PDI8-CN_2 thin films through polarization-resolved SHG (PR-SHG) we evidenced the occurrence of a finite three-dimensional PDI8-CN_2 region where the distribution of charge carriers lacks inversion symmetry and whose spatial profile is influenced by the HMDS treatment of SiO_2. An interpretation model is developed and presented, based on the Debye–Huckel charge screening mechanism triggered by charges localized in the SiO_2 dielectric layer. Such a picture, confirmed by photoluminescence findings, strengthens the hypothesis that proton migration in SiO_2 can account for the BSE effect in n-channel OFET also.

The work is organized as follows: the experimental methods and details are described in section 2; section 3 is devoted to the experimental results, involving PR-SHG and excitation-resolved photoluminescence (PLE) analysis and these are discussed in section 4. In section 5 we develop and discuss the interpretation model, while the main conclusions are finally drawn in section 6.

2. Experimental methods and details

Experimental investigation in the present work was carried out on two sets of PDI8-CN_2 thin films deposited on 200 nm-thick SiO_2 layers thermally grown on commercial (001) silicon substrates. In the first set, pristine Si/SiO_2 substrate was used for the deposition, while in the second set the SiO_2 surfaces were treated with HMDS. Each set consisted of six PDI8-CN_2 thin film samples with different thicknesses (d). Values for d were 6 nm, 10 nm, 20 nm, 42 nm, 70 nm and 102 nm for both pristine and HMDS-treated Si/SiO_2 substrates. Samples are indicated hereafter as S1 to S6 (according to increasing thickness).

The PDI8-CN_2 powder was purchased from Polyera Corporation Inc. (Polyera ActivInkTM N1200) and deposited by vacuum sublimation on the Si/SiO_2 substrates. Depositions were performed at a growth rate of 6 Å min^{-1} by a high-vacuum system (base pressure between 10^{-8} and 10^{-7} mbar) equipped with a Knudsen cell and a quartz microbalance. The chamber was warmed at temperature T=90° during deposition. Post-growth morphological characterization of films was performed by means of a XE100 Park atomic force microscope operating in air. Chemical functionalization by HMDS monolayer coverage was performed according to procedures elsewhere described [37].

Prior to PR-SHG analysis, PL and PLE spectroscopy measurements were performed on samples in order to gain information on optical transition levels and on the presence of near band-edge states in PDI8-CN_2 films: as discussed in section 4, such information is helpful to interpret the SHG experimental results. The PL and PLE analysis was performed by using a computer-controlled motorized system composed of a broad-band emission Xe lamp coupled with a monochromator equipped with 1200 grooves/mm double-grating, providing wavelength-tunable monochromatic optical excitation. PL emission was collected through a confocal lens system and focused onto the input slit of a 320 mm focal length spectrometer. The PLE signal was determined as the total PL emission (i.e. photoluminescence intensity spectrum integrated over emission photon energy) obtained as a function of excitation photon energy.

PR-SHG analysis was performed in reflection geometry (angle of incidence of about 45° by using a Nd:YAG mode-locked laser (emission wavelength λ_ω = 1064 nm, 20 ps pulses duration, 10 Hz repetition rate) as the fundamental beam. The polarization angle α of the linearly-polarized laser beam was varied through a 1064 nm half-wave retardation plate mounted on computer-controlled motorized rotation stage. Sharp cut-off optical filters were used to block fundamental beam reflected by the sample and the undesired residual SH wave generated in the various optical elements composing the setup. The p-polarized component of the SH output beam was selected by rotating a half-wave retardation plate operating at SH wavelength ($\lambda_{2\omega}$= 532 nm) and placed before a fixed polarizer. Finally, the output radiation was spectrally filtered at the SH wavelength by a PC-controlled motorized monochromator in order to remove any eventual spurious signal. A photomultiplier tube was used for SHG intensity detection. Each experimental point was obtained by averaging the SHG signal over 400 laser shots.

3. Experimental results

PL and PLE characterizations were performed with the experimental setup previously described. The excitation photon energy E (excitation wavelength λ) in PLE analysis was varied from E = 1.98 eV (λ = 625 nm) to E = 2.5 eV (λ = 496 nm) thus scanning the energy range from sub-bandgap to interband (i.e. HOMO–LUMO [38]) transition energies. Similar PL spectral features were observed in all samples, namely a broad emission spectrum approximately peaked at E = 1.85 eV and whose profiles were not symmetric with respect to their centre.

Representative peak-normalized PL spectra are reported in figure 1 (solid black curves) for samples S3 (top panel, 2A), S4 (middle panel, 2B) and S5 (bottom panel, 2C). It can be recognized that the centre-of-mass of the emission profile does not coincide with the peak position, suggesting therefore the presence of more than a single PL band. Excitation spectra obtained by PLE measurements are reported in figure 1 as open circles. To help comparison between the different plots, vertical dotted lines have been inserted to mark the energy positions of the excitation edge (E_0) and of the first excitation resonance (corresponding to optical absorption peaks) indicated as E_1. It is worth underlining that no significant sample-to-sample variation in the latter values is evidenced. The occurrence of an asymmetric PL profile (with the likely presence of double emission bands), the relevant spectral red-shift between the PL peak and the absorption edge and the partial overlap between the high-energy tail of PL emission and the absorption edge will be useful to sketch a scheme for the distribution of occupied electronic levels in PDI8-CN_2 films, supporting in turn the interpretation of SHG data.

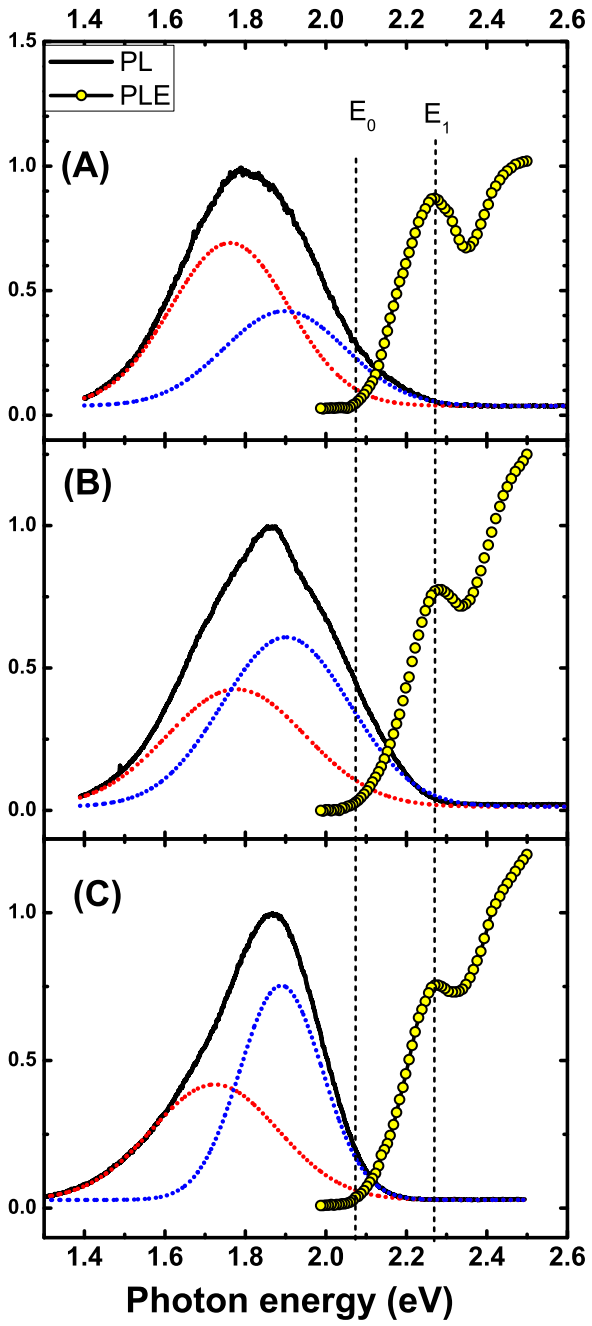

Figure 1. Peak-normalized PL (black curves) and PLE (yellow circles, arbitrary units) spectra of samples S3 (panel A), S4 (panel B) and S5 (panel C). The dotted curves are the Gaussian component used to decompose the PL spectra, obtained by double-Gaussian best fit of the PL data. To help comparison, the approximate energy positions of the excitation onset ($E_0 \approx 2.08$ eV) and of the first excitation resonance ($E_1 \approx 2.28$ eV) are marked by vertical dashed lines.

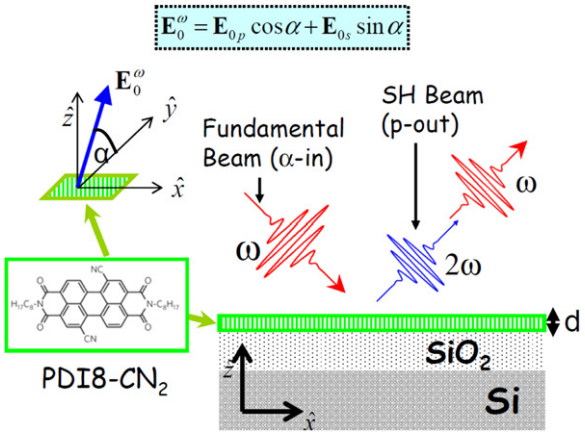

Figure 2. Schematic representation of the SHG experiment geometry. The fundamental beam of frequency ω impinges on the sample at an angle of incidence θ. The reflected fundamental beam and SH beam are both represented in the figure, where in the actual experimental setup the former is cut off by a suitable optical filter. The sample surface and plane of incidence are parallel to the xy and xz planes respectively. The polarization angle α is defined as the angle formed by the polarization direction of the fundamental electric field and the horizontal xy plane. In the green frame the structural formula of the PDI8-CN_2 molecule is reported.

The PR-SHG experiment geometry is represented in figure 2, showing the polarization angle α (defined as the angle between the polarization direction of the linearly-polarized fundamental electric field $\mathbf{E}_{\omega}$ and the sample surface) and the cartesian axis system used to describe the SHG signal. The experiments were performed by detecting the optical intensity of the reflected p-polarized (i.e. parallel to the plane of incidence xz in figure 3) SH wave as a function of the polarization angle α. The general purpose of the PR-SHG approach is to extract the individual SHG susceptibilities (i.e. tensor elements of the $\chi^{(2)}$ tensor that drives the SHG process) from experimental data. In the case of isotropic media, the $\chi^{(2)}$ tensor is composed by only three independent non-null elements, namely χ_{zzz}, χ_{zxx} and χ_{xxz}. Using the axis representation shown in figure 3, the polar pattern of p-polarized SHG intensity $I_P \propto |E_x|^2 + |E_z|^2$ vs α (indicated also as 'αp plot') can be directly related to the non-null susceptibility elements as follows:

$$I_p^{2\omega}(\alpha) \propto \left(I_{\omega}\sin\theta\right)^2 \cdot \left|A\sin^2\alpha + B\right|^2 \tag{1}$$

where $B = \chi_{zxx}$: therefore, the χ_{zxx} coefficient can be singled out through a best-fit of αp plots. It has to be noted that the coefficient A tangles together the non-null $\chi^{(2)}$ tensor elements, and therefore phase-resolved SHG measurements are also necessary to single out all of the tensor elements in the most general case [39]. However, this is not needed here, as we can obtain the necessary information from the χ_{zxx} coefficient only.

In figures 3(a) and 4(a) (upper panels) the experimental αp plots obtained for PDI8-CN_2 films deposited on pristine and HMDS-treated SiO_2 are reported, respectively, for some of the investigated samples (to improve the readability of the graphs, the αp curves for the S3 and S6 samples in figure 3(a) and for the S6 sample in figure 4(a) are omitted). Best-fit curves obtained by using equation (1) are reported as solid curves, while the corresponding best-fitting values

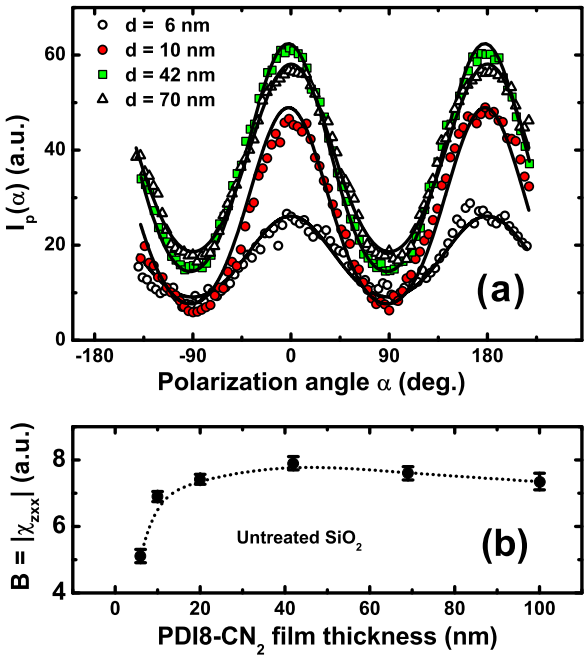

Figure 3. (a): α-in/p-out SHG intensity for PDI8-CN_2 films deposited on pristine SiO_2 (samples S1, S2, S4 and S5). Full lines represent the best-fit curves obtained by using equation (1). (b): $|\chi_{zxx}|$ susceptibility obtained by best fit of PR-SHG α-in/p-out data using equation (1) vs PDI8-CN_2 film thickness. The dotted line is a guide to the eye.

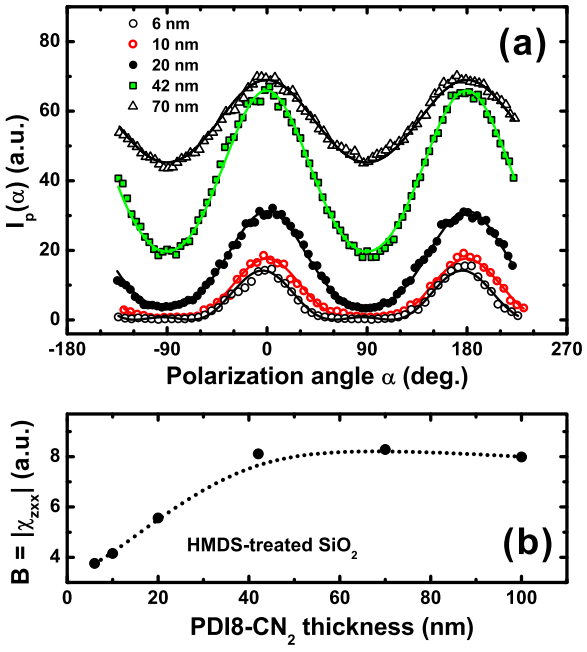

Figure 4. (a): α-in/p-out SHG intensity for PDI8-CN_2 films deposited on HMDS-treated SiO_2 (samples S1, S2, S3, S4 and S5). Full lines represent the best-fit curves obtained by using equation (1). (b): $|\chi_{zxx}|$ susceptibility obtained by best fit of PR-SHG α-in/p-out data using equation (1) vs PDI8-CN_2 film thickness. The dotted line is a guide to the eye.

for the $|B| = \left|\chi_{zxx}\right|$ susceptibility coefficient are shown in figures 3(b) and 4(b) as a function of PDI8-CN_2 film thickness.

All of the investigated PDI8-CN_2 films indeed exhibited the same αp polar pattern, in accordance with equation (1), representative of an average isotropic symmetry extended over the size of the optical interaction spot. Observation of such planar isotropy was indeed predictable, after considering that the optical excitation probes a surface area including a very high number of elongated domains with random in-plane orientation.

It can be seen that the SHG susceptibilities of both untreated and HMDS-treated SiO_2 exhibit a peculiar behavior, characterized by a thickness dependence at smaller film thicknesses followed by a plateau as the film thicknesses increase. Remarkably, the spatial profile and the characteristic 'saturation length' of the thickness-dependent SHG susceptibility is found to be affected by HMDS treatment of the SiO_2 surfaces. In order to understand these experimental findings, some considerations are drawn in the next section.

4. Discussion

The results shown in figures 3(b) and 4(b) indicate that the probed 'SHG-active' non-centrosymmetric region is not confined to 1–2 molecular layers only but extends instead for several nanometres, defining a finite volume above which a saturation of SHG amplitude is observed. Actually, SHG-active regions in centrosymmetric semiconductors can occur not only at material discontinuities, but also at finite internal regions characterized by the presence of electrostatic fields having a well-defined direction. This latter case, known as electric field-induced SHG (EFISHG), will be invoked in the next section to interpret the experimental results. Before elucidating the model in detail, we highlight in the present section some elements and qualitative evidences that will support our interpretation.

Even if no specific studies on the nature of PL-active states in PDI8-CN_2 are available, interesting considerations can be nevertheless expounded from our PL and PLE findings. To this aim, it is worth citing a recent *in situ* PL analysis performed on molecular films of perylene cores [41] evidencing room-temperature spectral contributions originating from excimer states and from defect states, where the former is significantly red-shifted ($\Delta E \approx 540$ meV) with respect to the 0–0 monomer transition [40, 42]. These results are very close to the ones here reported for PDI8-CN_2, whose PL also can be decomposed as a superposition of two contributes, one approximately peaked at $E_a = 1.76$ eV and another at about $E_b = 1.90$ eV. It is to be noted that the energy distance between E_a and the first absorption transition (E_1) is $\left|E_1 - E_a\right| \approx 520$ meV, almost equal to the result reported by Chen and Richardson [40]. We also underline that the second emission band occurs at photon energies very close to the onset of optical absorption E_0 evidenced by the PLE spectra. On these bases, the PL components peaked at energies E_a and E_b can be reasonably assigned to excimer emission and below-bandgap defective states, similarly to reference [40]. This allows to sketch a scheme for PDI8-CN_2 state occupation at equilibrium in which defect states accumulating below the LUMO edge are predominantly occupied and absorption transitions at photon energies below the E_0 edge are prevented by state-filling (i.e. the Pauli exclusion principle). In this situation, electrons occupying defective states below the LUMO edge and near band-edge states slightly above E_0 can recombine with holes created by supra-bandgap optical excitation, thus explaining why the

near band-edge transitions at photon energies less than E_0 are observed in emission spectra and not in excitation spectra.

The above described scheme for near band-edge state occupancy implies a Fermi level close to the LUMO edge and, as a consequence, a non-negligible occupation of LUMO states at finite temperature. This supports the presence of mobile electrons able to spatially redistribute themselves in as-grown PDI8-CN_2 films.

Other recent literature works also support the above conclusion. Very direct evidence of LUMO occupation was obtained by recent ultraviolet photoemission spectroscopy investigations evidencing a Fermi level positioned very close to the LUMO edge in PDI8-CN_2 films [43].

Furthermore, even stronger evidence can be exhibited supporting the presence of mobile electrons, namely the observation of negative threshold voltages (Vth) in OFETs based on PDI8-CN_2 using non-passivated SiO_2 as a gate dielectric [36]. This reveals that mobile electrons giving rise to source–drain current are present even at null gate voltages, and equivalently that negative gate voltages are needed to deplete the FET channel from already present mobile electrons.

Concerning the SHG results reported in figures 3 and 4, previous investigations [36] show that the HMDS treatment of SiO_2 substrates does not influence significantly the morphology of thermally-evaporated PDI8-CN_2 films, nor does it affect the optical parameters of the deposited films (refractive index and extinction coefficient) which depend on the specific molecule and on the molecular packing only. Therefore, it is not likely that the different thickness-dependent SHG patterns exhibited by film deposited on pristine (figure 3(b)) and HMDS-treated (figure 4(b)) SiO_2 surfaces can be attributed to linear optical effects. Moreover, the thickness dependence in SHG outlines the occurrence of a volume effect, suggesting that the observed nonlinear response cannot be assigned to interface polarization only. Finally, an eventual SHG dependence on film thickness due to optical interference between two SH waves generated at the film surface and the interface is also not likely for two reasons, namely: a) such an effect should lead to sinusoidal oscillatory behavior of SHG efficiency, which is not observed, and—even more importantly—b) this would not explain the differences in the results shown in figures 3(b) and 4(b), as HMDS treatment of SiO_2 does not modify the optical path in bulk PDI8-CN_2.

5. Interpretation model

Based on the experimental evidence and on the considerations reported in the previous section, a reasonable interpretation of our experimental data should: a) consider SHG-active regions not solely limited to the interface; b) explain the role of HMDS passivation in modifying the spatial profile of the SHG-active region; and c) include the presence of mobile charge, evidenced by both electrical and optical analyses, as a key ingredient.

Bearing in mind these considerations, we develop and discuss a possible interpretation model, based on the occurrence of the EFISHG phenomenon. EFISHG is driven by the third-order nonlinear susceptibility tensor $\chi^{(3)}$: being an odd-order term, $\chi^{(3)}$ is not restricted by inversion symmetry considerations and is therefore non-vanishing in the bulk of centrosymmetric media [44]. The EFISHG term arises from the local presence of a static electric field (indicated by $\mathbf{E}^{dc}(z)$) giving rise to a nonlinear polarization whose expression (using tensor

notation) is [45, 46] $\mathbf{P}_{2\omega}^{(EFISHG)} = \chi^{(3)} : \mathbf{E}^{\omega}\mathbf{E}^{\omega}\mathbf{z} \cdot E^{dc}(z)$, where $\mathbf{E}^{dc}$ is assumed to be directed along the normal to the material surface due to the isotropy of the system in the *xy* plane.

For the present model, we derived the expression of the total effective SHG susceptibility for an isotropic film in the presence of both interfacial and electric field-induced SHG by using the Green function formalism developed by Sipe for surface optics [47]. The calculation details are reported in the Supporting Information section, where the following expression is demonstrated:

$$\chi_{zxx} = \chi_{zxx}^{(I)} + \gamma_3 \exp(-d/\Lambda) \times F(d). \tag{2}$$

Here, d is the semiconductor thickness, $\chi_{zxx}^{(I)}$ is the interfacial second-order nonlinear susceptibility and γ_3 is the *zxxz* element of the $\chi^{(3)}$ tensor element. The actual spatial profile of the internal electrostatic field and the semiconductor thickness affect the effective SHG susceptibility through the term $F(d)$, whose expression is:

$$F(d) = \int_0^d E^{dc}(z) \exp\left[-iz/L_C\right] dz \tag{3}$$

where $L_C = \lambda_\omega / 4\pi \left(n_\omega \cos\theta_\omega + n_{2\omega} \cos\theta_{2\omega}\right)$, θ_i $(i = \omega, 2\omega)$ is the refraction angle of fundamental $(i = \omega)$ and SH wave $(i = 2\omega)$ in the sample, n_i is the PDI8-CN_2 refractive index at the fundamental wavelength (λ_ω) and SH wavelength $(\lambda_{2\omega})$. Finally, $\Lambda = \lambda_{2\omega}/2\pi\kappa_{2\omega} \cos\theta_{2\omega}$, where $\kappa_{2\omega}$ is the extinction coefficient of PDI8-CN_2 at the SH wavelength.

The presence of a net uncompensated charge localized about the SiO_2/PDI8-CN_2 interface can account for the peculiar behaviour obtained for SHG susceptibility $|\chi_{zxx}|$. To demonstrate this, we underline that the organic molecules in our SHG experiments are in the neutral state (no external bias is applied): as a consequence, any eventual accumulation of localized charge has to be compensated by redistribution of opposite charge in order to guarantee the overall charge neutrality. Such a redistribution will give rise to a built-in electric field $E^{dc}(z)$ that screens out the unbalanced local charge, contributing also to an EFISHG term in the total SHG response (see equations (2) and (3)).

The spatial profile $E^{dc}(z)$ of the electrostatic field is of course ruled by the Poisson equation that, in the general case, has to be solved numerically [48, 49] due to its intrinsic non-linear nature (i.e. the charge density ρ itself depends on the local value of electrostatic potential ϕ). However, a simplified analytical expression for $E^{dc}(z)$ can be obtained under the assumption of the Debye–Huckel approximation, consisting of a linearization of the ρ vs ϕ dependence. In the case of a non-degenerated n-type semiconductor at temperature T, such approximation leads to an exponentially-decaying built-in electric field characterized by a screening length L_D [50]:

$$E^{dc}(z) = E_0^{dc} \exp\left(-z/L_D\right). \tag{4}$$

In spite of its simplicity, the above expression for the electric field takes into account the main features observed for SHG susceptibilities of PDI8-CN_2. In fact, using equations (3) and (4) the field-dependent quantity $F(d)$ becomes:

$$F(d) = \int_0^d E_0^{dc} \exp\left[-z\left(L_D^{-1} + iL_C^{-1}\right)\right] dz. \tag{5}$$

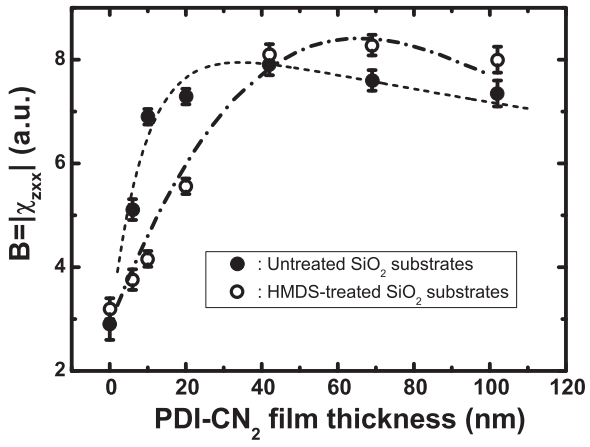

Figure 5. Full circles: $|\chi_{zxx}|$ SHG susceptibility obtained by PR-SHG analysis of the PDI8-CN_2 films grown on untreated SiO_2 (full circles) and HMDS-treated SiO_2 (open circles). Curves: best fit of experimental data (dashed curve: films grown on untreated SiO_2, fit performed through equation (6); dot-dashed curve: films grown on HMDS-treated SiO_2, fit performed through the analytic expression).

It is easily seen that the modulus of equation (5) describes a thickness-dependent quantity that increases for $d < L_D$, followed by saturation and attenuation as film thickness approaches the attenuation length Λ, thus reproducing the results determined experimentally (see figures 3(b) and 4(b)).

A simple expression for χ_{zxx}^{tot} can be obtained in the case where the built-in electric field extends up to a screening length L_D less than the SHG coherence length L_C: using a first-order Taylor approximation ($\exp\left[-iz/L_C\right] \cong 1$) we obtain:

$$\chi_{zxx}^{tot} = \chi_{zxx}^{(I)} + \gamma_3 L_D E_0^{dc} \exp\left(-d/\Lambda\right)\left(1 - \exp\left(-d/L_D\right)\right). \tag{6}$$

In case the extent of the built-in electric is comparable or even larger than the coherence length, the integral (5) can be analytically performed, whose square modulus describes the $|\chi_{zxx}|(d)$ (see equation (2)). Ellipsometric analysis of PDI8-CN_2 (not reported here) allowed us to estimate a coherence length of about 29 nm: we therefore used the exact expression for $|\chi_{zxx}|(d)$ to fit the data referring to samples grown on passivated substrates (as they clearly exhibit a larger 'saturation length'), while the use of the approximated expression (equation (6)) is sufficient for the first set of samples (untreated substrates).

The obtained results are reported in figure 5, where full circles and a dashed line represent the experimental data (obtained by PR-SHG analysis, equation (1)) and the best-fit curves, respectively. A good qualitative agreement between the experimental data and the model prediction is evidenced, obtaining values of about 0.6 ± 0.2 (untreated SiO_2) and 0.19 ± 0.6 (HMDS-treated SiO_2) for $\gamma_3 E_0^{dc}$ and of 10 ± 2 nm and 60 ± 10 nm for the screening lengths L_D (untreated and HMDS-treated SiO_2, respectively). Even if the fitting parameters are clearly not very accurate due to scarce statistics, we underline that L_D is ultimately a phenomenological parameter used to describe the charge-screening mechanism is a simple way. Therefore, physically relevant conclusions can be expounded regardless of its actual exact value.

Inspection of equation (6) shows that the initial slope of $\chi_{zxx}^{tot}(d)$ is dictated by the $\gamma_3 E_0^{dc}$ term (i.e. $\chi_{zxx}^{tot}(d) \cong \chi_{zxx}^{(I)} + \gamma_3 E_0^{dc} d$ for small d values). As it is unreasonable that the bulk

susceptibility γ_3 is affected by substrate treatment, the lesser slope exhibited by samples grown on HMDS-treated substrates suggests that HMDS coverage reduces the electrostatic field (and, in turn, the local electrostatic charge) just about at the SiO_2 interface with the organic layer. Furthermore, the longer screening length obtained for samples grown on HMDS-treated substrates suggests these latter are characterized by a lesser concentration of mobile charges, so that a larger volume is needed to screen out the charge immobilized at the SiO_2 surface[5]. In short, experimental findings suggest a role of SiO_2 passivation in reducing the amount of immobilized and mobile charge at the interface with the gate dielectric and in the semiconductor.

Taking into account the hydrophobic effect exerted by HMDS treatments of SiO_2 surfaces, an interesting conclusion can be drawn regarding the role of water in operational instabilities of n-channel OFETs. To explain the BSE in p-channel OFETs using SiO_2 as a gate dielectric, Bobbert and coworkers proposed a mechanism based on proton migration from the surface toward the bulk of SiO_2 [35]. In their model, the presence of adsorbed water molecules on SiO_2 surfaces plays a key role, initiating redox reactions that involve holes in the semiconductor, water, oxygen and protons [51, 52] and leading to the establishment of an equilibrium between the surface concentration of holes in the accumulation layer and the density of protons in SiO_2 close to the surface. Successive proton diffusion in SiO_2 thus induces the reduction of threshold-voltage shift as a function of time observed in BSE.

This mechanism allows one to explain the major features characterizing the BSE in p-type OFETs and sets up an issue regarding whether a proton diffusion mechanism is involved for both p-type and n-type BSE. To this regard, Bobbert and coauthors also suggested that in n-channel OFETs an equilibrium exists—even before eventual application of a gate bias—between negatively charged Si-O groups on the SiO_2 surface (resulting from the hydrolysis of surface silanol groups Si-OH [53]) and protons in the SiO_2 [36]. In such a case, application of a positive bias to the n-channel OFET will lead to proton drift from SiO_2 towards the semiconductor, removal of electrons from the semiconductor and BSE.

Our investigations support this latter picture. In fact, the presence of negatively charged $Si\text{-}O^-$ groups present even at null gate bias can account for the interface fixed charge initiating the screening field and EFISHG polarization. HMDS treatments act by reducing the surface concentrations of the silanol groups and of the adsorbed water molecules [51], thus leading to the decrease in the density of immobilized charge also deduced from our SHG analysis. Moreover, mobile (bulk) charge concentration is also decreased by hydrophobic passivation, as indicated by the reduction of source–drain current at null bias voltage in PDI8-CN_2 OFETs [37]. To explain this, a reaction leading to the reduction of organic molecules and involving water and oxygen has been suggested as follows: $2\,H_2O + 4os \rightleftharpoons 4\,H^+ + 4os^- + O_{2(solv)}$ (where os stands for the organic semiconductor). Reduced organic molecules (os^-) can account for the mobile charge responsible for the source–drain current at null gate bias and for the build-up of the screening field $E^{dc}(z)$ involved in EFISHG contribution. According to this reaction,

[5] Indeed, in rigorous Debye-Huckel screening in which the interface band bending is not larger than few k_{BT}'s and the local charge is fully screened, the screening length depends only on the bulk concentration of mobile charge, according to $L_D = \sqrt{\epsilon k_B T / 8\pi e^2 n_b}$, being n_b and k_B the bulk density of mobile charge carriers and the Boltzmann constant, respectively. However, in our case the amount of charge to be screened is also likely to depend on SiO_2 treatment, so it is not obvious that a quantitative conclusion about the total bulk density of charge can be inferred by simply comparing the different screening lengths obtained for the two sets of samples.

hydrophobic treatment will also decrease the mobile charge density (or, equivalently, increase the screening length) again in agreement with the experimental findings.

6. Conclusions

In conclusion, in this work we investigated the possibility to employ optical second-harmonic generation as a technique to perform contact-free and spatially-selective probing of electronic distribution in PDI8-CN_2 molecular films deposited on SiO_2 dielectric layers. In particular, we sought evidence of inversion symmetry-breaking charge distribution at the buried PDI8-CN_2/SiO_2 interface and/or in the organic semiconductor layer, through analysis of SHG dielectric susceptibilities in PDI8-CN_2 films of variable thickness and deposited on untreated and HMDS-treated SiO_2 layers. In all investigated cases the results pointed out a finite three-dimensional 'SHG-active' semiconductor region in which spatial distribution of charge carriers lacked inversion symmetry, suggesting the presence of an internal built-in electrostatic field that leads to an additional contribution to SHG. Experimental findings are modeled in terms of electric field-induced SHG phenomenon initiated by net charges lying at the top of the SiO_2 gate dielectric layer and inducing a non-uniform charge distribution (or, equivalently, a Debye-like screening field) in bulk PDI8-CN_2. SiO_2 surface passivation by HMDS has been found to play a relevant role in dictating the strength of the interface field and its spatial distribution. Photoluminescence and excitation-resolved photoluminescence characterizations have also been performed, supporting the presence of mobile charge carriers in PDI8-CN_2 and reinforcing the proposed interpretation. The experimental results can be interpreted as a consequence of reduction–oxidation reactions involving PDI8-CN_2, water molecules and surface silanol hydrolysis. This supports the hypothesis that a 'universal' mechanism determines and rules the operation instabilities for both p-type and n-type OFETs, related to proton diffusion in bulk SiO_2.

References

[1] Ishii H, Sugiyama K, Ito E and Seki K 1999 *Adv. Mater.* **11** 605
[2] Braun S, Salaneck W R and Fahlman M 2009 *Adv. Mater.* **21** 1450
[3] Veres J, Ogier S D, Leeming S W, Cupertino D C and Mohialdin Khaffaf S 2003 *Adv. Funct. Mater.* **13** 199
[4] Stassen A F, de Boer R W I, Iosad N N and Morpurgo A F 2004 *Appl. Phys. Lett.* **85** 3899
[5] Hulea I N, Fratini S, Xie H, Mulder C L, Iossad N N, Rastelli G, Ciuchi S and Morpurgo A F 2006 *Nature Mater.* **5** 982
[6] Sirringhaus H 2009 *Adv. Mater.* **21** 3859
[7] Zilker S J, Detcheverry C, Cantatore E and de Leeuw D M 2001 *Appl. Phys. Lett.* **79** 1124
[8] Richards T and Sirringhaus H 2008 *Appl. Phys. Lett.* **92** 023512
[9] Sharma A, Mathijssen S G J, Smits E C P, Kemerink M, de Leeuw D M and Bobbert P A 2010 *Phys. Rev.* B **82** 075322
[10] Chen 10 Y and Podzorov V 2012 *Adv. Mater.* **24** 2679
[11] de Leeuw D M, Simenon M M J, Brown A R and Einerhand R E F 1997 *Synth. Met.* **87** 53
[12] Newman C R, Frisbie C D, da Silva Filho D A, Brdas J-L, Ewbank P C and Mann K R 2004 *Chem. Mater.* **16** 4436
[13] di Pietro R and Sirringhaus H 2012 *Adv. Mater.* **24** 3367
[14] di Pietro R, Fazzi D, Kehoe T B and Sirringhaus H 2012 *J. Am. Chem. Soc.* **134** 14877
[15] Butcher P N and Cotter D 1991 *The Elements of Nonlinear Optics* (Cambridge: Cambridge University Press)

[16] Lettieri S, Gesuele F, Maddalena P, Liscidini M, Andreani L C, Ricciardi C, Ballarini V and Giorgis F 2005 *Appl. Phys. Lett.* **87** 191110
[17] Lettieri S, Merola F, Maddalena P, Ricciardi C and Giorgis F 2007 *Appl. Phys. Lett.* **90** 021919
[18] Chang Y M, Xu L and Tom H W K 1997 *Phys. Rev. Lett.* **78** 4649
[19] Guo C, Rodriguez G and Taylor A J 2001 *Phys. Rev. Lett.* **86** 1638
[20] Hoffmann T, Thielen P, Becker P, Bohat L and Fiebig M 2011 *Phys. Rev.* B **84** 184404
[21] Manaka T, Lim E, Tamura R and Iwamoto M 2007 *Nature Photon.* **1** 581
[22] Manaka T, Nakao M, Lim E and Iwamoto M 2008 *Appl. Phys. Lett.* **92** 142106
[23] Lim E, Lee H, Manaka T and Iwamoto M 2008 *Japan. J. Appl. Phys.* **47** 3179
[24] Tanaka Y, Manaka T and Iwamoto M 2011 *Chem. Phys. Lett.* **507** 195
[25] di Girolamo F V, Barra M, Chiarella F, Lettieri S, Salluzzo M and Cassinese A 2012 *Phys. Rev.* B **85** 125310
[26] Jones B A, Ahrens M J, Yoon M H, Facchetti A, Marks T J and Wasielewski M R 2004 *Angewandte Chemie International Edition* **43** 6363
[27] Jones B A, Facchetti A, Wasielewski M R and Marks T J 2008 *Adv. Funct. Mater.* **18** 1329
[28] Yoo B, Madgavkar A, Jones B A, Nadkarni S, Facchetti A, Dimmler K, Wasielewski M R, Marks T J and Dodabalapur A 2006 *IEEE Electron Device Lett.* **27** 737
[29] Rivnay J, Jimison L H, Northrup J E, Toney M F, Noriega R, Lu S, Marks T J, Facchetti A and Salleo A 2009 *Nature Mater.* **8** 952
[30] Liscio F, Milita S, Albonetti C, D'Angelo P, Guagliardi A, Masciocchi N, della Valle R G, Venuti E, Brillante A and Biscarini F 2012 *Adv. Funct. Mater.* **22** 943
[31] Flytzanis C 1995 Nonlinear polarization *Optical and Non-linear Materials: Principles and Applications (Proceedings of the International School of Physics 'Enrico Fermi')* (Amsterdam: IOS)
[32] Mathijssen S G J, Kemerink M, Sharma A, Clle M, Bobbert P A, Janssen R A J and de Leeuw D M 2008 *Adv. Mater.* **20** 975
[33] Gomes H L, Stallinga P, Clle M, de Leeuw D M and Biscarini F 2006 *Appl. Phys. Lett.* **88** 082101
[34] Gomes H L, Stallinga P, Dinelli F, Murgia M, Biscarini F, de Leeuw D M, Muck T, Geurts J, Molenkamp L W and Wagner V 2004 *Appl. Phys. Lett.* **84** 3184
[35] Kalb W, Mathis T, Haas S, Stassen A and Batlogg B 2007 *Appl. Phys. Lett.* **90** 092104
[36] Bobbert P A, Sharma A, Mathijssen S G J, Kemerink M and de Leeuw D M 2012 *Adv. Mater.* **24** 1146–58
[37] di Girolamo F V, Ciccullo F, Barra M, Carella A and Cassinese A 2012 *Organic Electronics* **13** 2281
[38] Chiarella F, Barra M, Cassinese A, di Girolamo F, Maddalena P, Santamaria L and Lettieri S 2011 *Appl. Phys. A: Mater. Sci. Process.* **104** 39
[39] Corn R M and Higgins D A 1994 *Chem. Rev.* **94** 107
[40] Zhang T G, Zhang C H and Wong G K 1990 *J. Opt. Soc. Am. B* **7** 902
[41] Chen Q and Richardson N V 2010 *J. Phys. Chem.* C **114** 6062
[42] Nishimura H, Yamaoka T, Mizuno K, Iemura M and Matsui A 1984 *J. Phys. Soc. Japan* **53** 3999
[43] Chua L L, Ƶaumseil J, Chang J F, Ou E C W, Ho P K H, Sirringhaus H and Friend R H 2005 *Nature* **434** 194
[44] Lee C H, Chang R K and Bloembergen N 1967 *Phys. Rev. Lett.* **18** 167
[45] Shen Y R 2002 *The Principles of Nonlinear Optics* (New York: Wiley-Interscience)
[46] Aktsipetrov O A, Fedyanin A A, Golovkina V N and Murzina T V 1994 *Opt. Lett.* **19** 1450
[47] Sipe J E 1987 *J. Opt. Soc. Am.* B **4** 481
[48] Mayergoyz I D 1986 *J. Appl. Phys.* **59** 195
[49] Pacelli A 1997 *IEEE Trans. Electron Devices* **44** 1169
[50] Luth H 2010 *Solid Surfaces Interfaces and Thin Films* 5th edn (Berlin: Springer)
[51] Sharma A, Mathijssen S G J, Kemerink M, de Leeuw D M and Bobbert P A 2009 *Appl. Phys. Lett.* **95** 253305
[52] Sharma A, Mathijssen S G J, Smits E C P, Kemerink M, de Leeuw D M and Bobbert P A 2010 *Phys. Rev.* B **82** 075322
[53] Chua L L, Zaumseil J, Chang J F, Ou E C W, Ho P K H, Sirringhaus H and Friend R H 2005 *Nature* **434** 194